JETIR.ORG ISSN: 2349-5162 | ESTD Year : 2014 | Monthly Issue

JOURNAL OF EMERGING TECHNOLOGIES AND INNOVATIVE RESEARCH (JETIR)

An International Scholarly Open Access, Peer-reviewed, Refereed Journal

Synthesis and Spectroscopic Properties of Dy^{3+} Activated $Li_2Zr(PO_4)_2$ Phosphor

Bhuneshwar Verma,[1*] V. Jena[2]

[1]Department of Physics, Govt. Nagarjuna PG College of Science, Raipur 492010, India

[2]Department of Chemistry, Govt. Nagarjuna PG College of Science, Raipur 492010, India

Abstract

In this work, a group of $Li_2Zr(PO_4)_2$ doped with various Dy^{3+} concentrations were prepared utilizing the solid state reaction method. The crystalline phases were identified by the implement of XRD as well as Rietveld refinement. The surface morphology, elemental analysis and vibrational properties were characterized by SEM, EDX and FTIR techniques. Upon the irradiation of 349 nm, all the phosphors exhibited blue-green light emission with the primary peak at 488 nm. Furthermore, the optimal doping concentration of Dy^{3+} ion was determined as 2 mol%, and the mechanism of energy transfer between two adjacent Dy^{3+} ions was dominated by the dipole-dipole interaction. The possible lattice sites occupied by Dy^{3+} ions were investigated via the fitting function type of decay curves. The calculated CIE chromaticity coordinate of $Li_2Zr(PO_4)_2$:Dy^{3+} (2 mol%) phosphor verified that its emission light was located in the blue-green region. The aforesaid results demonstrated that the $Li_2Zr(PO_4)_2$:Dy^{3+} phosphors could be potential candidates for application in display and solid state lighting.

Keywords: $Li_2Zr(PO_4)_2$:Dy^{3+}; XRD; Photoluminescence; Decay time.

1. INTRODUCTION

Solid-state lighting (SSL) with light-emitting diodes (LEDs) is the recent research focus in the lamp industry. The SSL technology has numerous advantages over conventional light sources for instance consumption of low power, compactness, efficient output and longer lifetime. The SSL would have its impact on reducing the comprehensive electricity consumption. LEDs have an immense prospect to substitute them and are considered as a subsequently invention solid state light devices [1, 2]. The phosphate based host matrices have greatly attracted for an widespread analysis because of their broad applications in optical

devices. In recent years, orthophosphates have become a significant host due to their outstanding thermal stability. In comparison with commercially accessible YAG: Ce^{3+} phosphor, the phosphate based $KSrPO_4$: Eu^{2+} and $KBaPO_4$: Ln (Ln = Eu^{2+}, Tb^{3+}, Sm^{3+}) phosphors exhibit higher thermally stable luminescence [3, 4]. The trivalent Dy^{3+} ions, which illustrate the luminescence spectrum in the 450 – 500 nm region owing to $^4F_{9/2}$ – $^6H_{15/2}$ transition and in the 570 – 600 nm region due to the $^4F_{9/2}$ – $^6H_{13/2}$ transition, have aroused a great interest among researchers due to its white light emission [5–7] as well as its spectra in visible region 400 − 600 nm have attracted much interest owing to its white light emission [8–11]. Out of many rare-earths (REs) ions, Dy^{3+} ions activated phosphors have normally been used as highly efficient activators showing their photoluminescence spectra ranging from 450 to 700 nm [12]. The luminescent efficiency can be enhanced significantly when phosphors are doped with appropriate auxiliary activators. In this study, the method for preparation of Dy^{3+} doped $Li_2Zr(PO_4)_2$ phosphors have been presented and its structural morphology, elemental composition, decay time and photo-luminescent properties have also been studied.

2. EXPERIMENTAL SECTION

In order to prepare the un-doped and Dy^{3+} doped $Li_2Zr(PO_4)_2$ phosphors, all raw materials including Li_2CO_3, ZrO_2 and $NH_4H_2PO_4$ were taken of analytical grade and Dy_2O_3 with 99.99% purity. The raw materials were thoroughly mixed and preheated at 200 °C for 5 h to decompose $NH_4H_2PO_4$, then at 900 °C for 5h to decompose Li_2CO_3, and finally heated at 1100 °C for 5h to transform meta-phosphate to orthophosphate. After that the temperature was slowly decreased down to room temperature. The synthesized phosphors $Li_2Zr(PO_4)_2$:Dy^{3+} were characterized by X-ray diffraction (XRD), scanning electron microscopy (SEM), energy dispersive X-ray (EDX) spectroscopy, Fourier transform infrared (FTIR) analysis. X- ray diffraction (XRD) pattern of $Li_2Zr(PO_4)_2$:Dy^{3+} phosphor was recorded using PANalytical X- ray diffractometer in the 2θ range from 10 to 80°, with the Cu target radiation having wavelength λ =1.5406 Å. The morphology and elemental composition of prepared phosphors was examined using a ZEISS-EVO 60 m scanning electron microscope (SEM). The excitation and emission spectra of the samples were recorded by using a RF-5301 PC Shimadzu spectrofluoro-photometer. The fluorescence decay times have been observed by using pico second time resolved (PSTR) fluorimeter.

3. RESULTS AND DISCUSSION

3.1 XRD analysis

Fig. 1 presents the XRD patterns of the prepared powder samples of un-doped and doped $Li_2Zr(PO_4)_2$:Dy^{3+} (2 mol%) phosphors**.** A small quantity of the doping of Dy^{3+} ions in the crystal does not affect the crystal structure. The patterns were compared with those of the standard JCPDS code: 38-0278 and which has matched well. Crystal structure refinement of the recorded XRD pattern was performed using PANalytical high score report. Refinement was done considering the hexagonal unit cell and space group R3C and space group number 167. The refined lattice parameters were found as a = b = 8.8370 Å, c = 22.4180 Å, α = 90°, β = 90°, γ = 120° and cell volume V = 1516.13 $Å^3$, Z = 6 and density was to be calculated 3.12 g/cm^3. The crystallite size (D_{hkl}) of the samples was calculated using Debye-Scherrer equation given as follows [13].

$$D_{hkl} = \frac{K\lambda}{\beta \cos\theta} \quad (1)$$

where, K is the Scherrer constant, λ is the wavelength of the X-ray used. Using equation (1), the values of D_{hkl} were calculated to be as 50.23 nm and 52.80 nm for un-doped and Dy^{3+} doped $Li_2Zr(PO_4)_2$ phosphors, respectively.

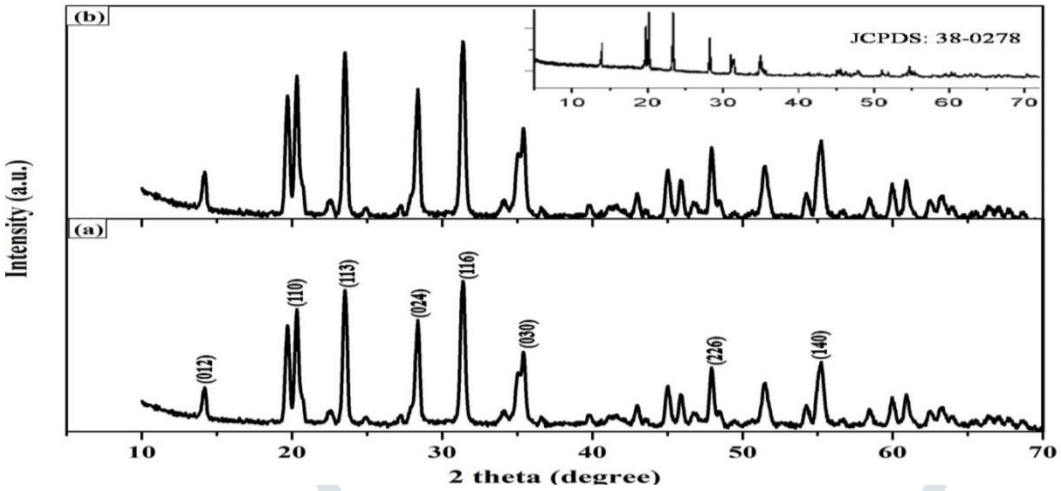

Fig. 1. XRD patterns of (a) un-doped and (b) $Li_2Zr(PO_4)_2$:Dy^{3+} phosphors.

3.2 Morphological and elemental analysis

The Scanning electron microscopy (SEM) was carried out to study the surface morphology of the sample and grain sizes of the prepared phosphor powder were calculated. The SEM images of the $Li_2Zr(PO_4)_2$ and $Li_2Zr(PO_4)_2$:Dy^{3+} (2 mol%) phosphors are demonstrated in Fig. 2. The SEM images obtained show a non-uniform surface without void or flaws which covered the substrate well. The surface morphology shows that the grains are composed of particle of slightly different sizes. The physical observation shows that sample of the pure $Li_2Zr(PO_4)_2$ and Dy^{3+} doped $Li_2Zr(PO_4)_2$ show agglomeration with slightly similar morphology having different sizes while doped one show irregular structure of different sizes.

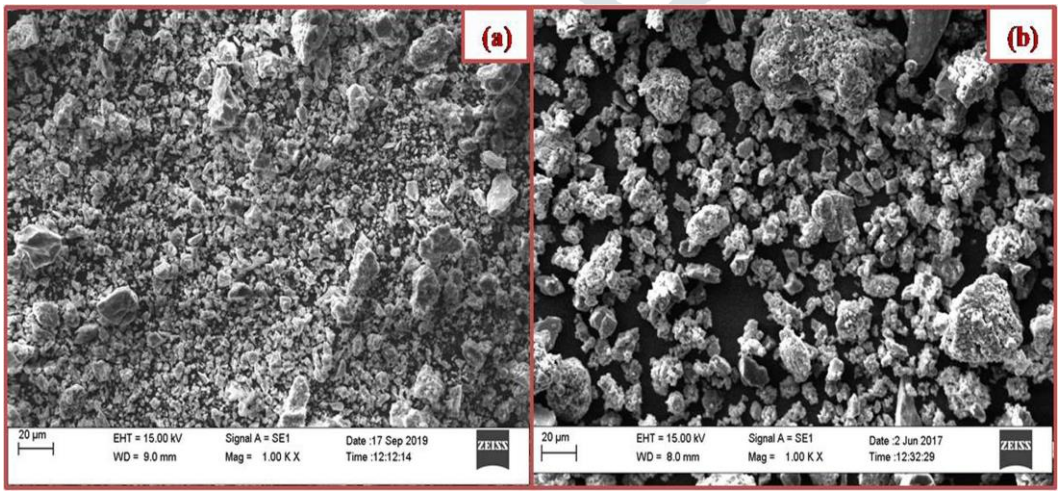

Fig. 2. SEM images of (a) un-doped and (b) $Li_2Zr(PO_4)_2$: Dy^{3+} phosphors.

Furthermore, the compositional results of un-doped and Dy^{3+} doped $Li_2Zr(PO_4)_2$ phosphors were examined and patterns are displayed in Fig. 3. The results show that the doped sample composed of the main element such as Zirconium (Zr), Phosphorus (P), Oxygen (O) and Dysprosium (Dy) with some traces of other elements. Lithium (Li) could not be detected by EDX measurement due to less atomic number [14]. The chemical compositions of elements for un-doped and Dy^{3+} doped samples are given in Table 1.

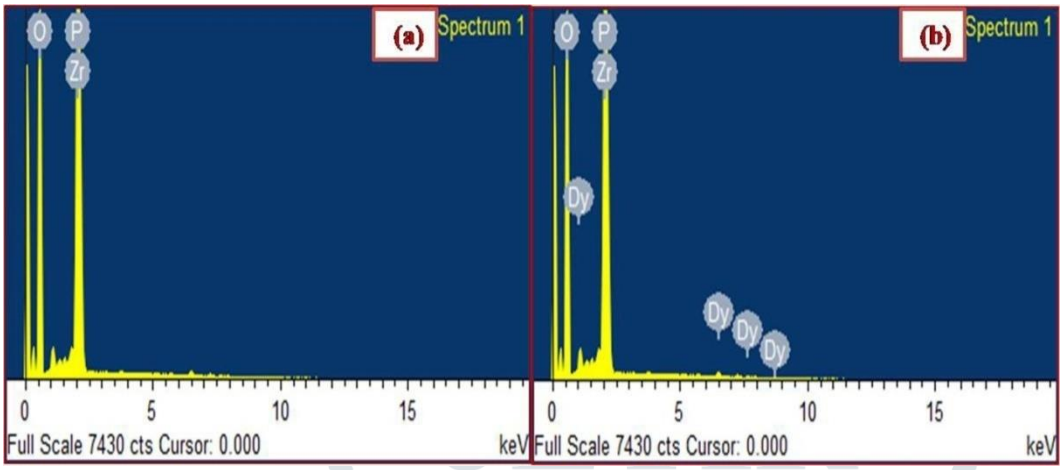

Fig. 3. EDX results of (a) un-doped and (b) $Li_2Zr(PO_4)_2$: Dy^{3+} phosphors.

Table 1. Composition of $Li_2Zr(PO_4)_2$ and $Li_2Zr(PO_4)_2$:Dy^{3+} phosphors.

(a) Undoped $Li_2Zr(PO_4)_2$

S. No.	Standard	Elements	Weight %	Atomic%
1	SiO_2	O K	57.96	80.33
2	GaP	P K	19.98	14.31
3	Zr_2	Zr L	22.06	5.36
	Total		**100.00**	**100.00**

(b) $Li_2Zr(PO_4)_2$: Dy^{3+} (2 mol%)

S. No.	Standard	Elements	Weight %	Atomic%
1	SiO_2	O K	56.55	79.89
2	GaP	P K	19.79	14.44
3	Zr_2	Zr L	21.82	5.41
4	DyF_3	Dy L	1.84	0.26
	Total		**100.00**	**100.00**

3.3 FTIR study

The vibrational properties of the synthesized phosphor were studied by Fourier transform infrared (FTIR) spectroscopy. The FTIR spectrum was recorded in the range of 4000 – 400 cm^{-1}. Typical FTIR spectrum of $Li_2Zr(PO_4)_2:Dy^{3+}$ (2 mol%) phosphor is depicted in Fig. 4. The broad peak centered at 3358 cm^{-1} is visible due to stretching of O−H bonds which supports the presence of moisture in the sample. A small peak originated at 2922 cm^{-1} is ascribed to filter contamination of the FTIR instrument. The band assigned to the 925- 406 cm^{-1} is due to the vibration of stretching modes of PO_4^{3-} groups and symmetric P-O-P bridge frequency [15, 16]. Thus, the obtained results suggest that the prepared matrix belongs to the meta-phosphate family.

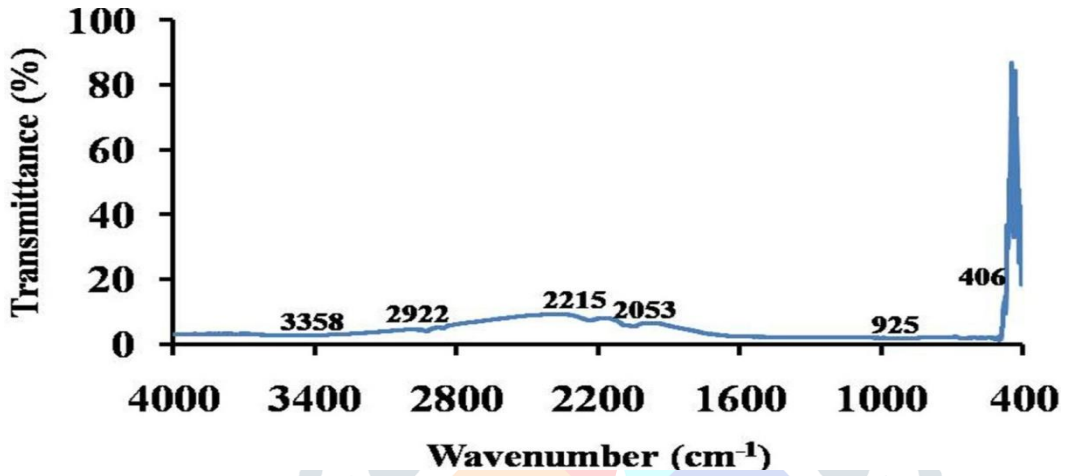

Fig. 4. FTIR spectrum of $Li_2Zr(PO_4)_2:Dy^{3+}$ (2 mol%) phosphor.

3.4 Photoluminescence (PL) properties

Fig. 5 depicts the PL excitation (PLE) spectrum of $Li_2Zr(PO_4)_2:Dy^{3+}$ (2 mol%) phosphor, monitored at emission wavelength (λ_{em}) of 483 nm. The two characteristic transitions of Dy^{3+} namely at 349 nm ($^6H_{15/2} \rightarrow {}^6P_{7/2}$) and 362 nm ($^6H_{15/2} \rightarrow {}^6P_{5/2}$) were observed. The most intense peak were obtained at 349 nm ($^6H_{15/2} \rightarrow {}^6P_{7/2}$). In turn, this wavelength can be employed to measure the photoluminescence emission spectra.

Fig. 6 shows the photoluminescence (PL) emission spectra of $Li_2Zr(PO_4)_2:xDy^{3+}$ (x = 0.5, 1, 2, 3 and 4 mol%) phosphors, which were recorded under 349 nm excitation wavelengths. The emission spectra of $Li_2Zr(PO_4)_2:Dy^{3+}$ exhibit two characteristic emission peaks at wavelength 488 nm (blue emission) and at 577 nm (yellow emission) which corresponds to the magnetic dipole (MD) transition $^4F_{9/2} \rightarrow {}^6H_{15/2}$ and the electric dipole (ED) transition $^4F_{9/2} \rightarrow {}^6H_{13/2}$ with respect to Dy^{3+} ion, respectively [17]. The excitation energy at 349 nm excites the Dy^{3+} ions to energy level $^6P_{7/2}$ and then these ions quickly relax to its lower excited energy level $^4F_{9/2}$ by the non-radiative transition which is further populated. The transitions of ions from $^4F_{9/2}$ energy level to energy levels $^6H_{15/2}$ and $^6H_{13/2}$ yield PL emission. The ED transition dominates in the emission spectra when Dy^{3+} ion is located at a low symmetry site and the MD transition is so when Dy^{3+} ion is located at high symmetry sites [18]. In $Li_2Zr(PO_4)_2:Dy^{3+}$ predominant emission is around 488 nm suggesting that ligand fields lightly deviates from its inversion symmetry [19].

Fig. 7 shows the intensity of PL emission peaks corresponding to the magnetic dipole (MD) transition $^4F_{9/2} \rightarrow {}^6H_{15/2}$ (488 nm) as a function of Dy^{3+} ions concentration. It is clear from the Fig 6 that magnetic dipole (MD) dominates over the electric dipole (ED) transition for all concentration of Dy^{3+} ions. It is also observed that blue emission $^4F_{9/2} \rightarrow {}^6H_{15/2}$ (488 nm) is stronger than yellow emission $^4F_{9/2} \rightarrow {}^6H_{13/2}$ (577 nm). The PL intensity initially increases with increasing Dy^{3+} concentration up to 2 mol%, whereas beyond the 2 mol% the intensity decreases due to concentration quenching. Concentration quenching depends upon the non-radiative energy transfer among Dy^{3+} ions. It also strongly depends upon the critical distance (R_c) between nearby ions. The critical distance (R_c) between the Dy^{3+} ions can be calculated using the relation given below [20].

$$R_c = 2\left(\frac{3V}{4\pi x_c Z}\right)^{\frac{1}{3}} \quad (2)$$

where V is the volume of the unit cell, Z is the number of activators in the unit cell and x_c is the critical concentration of activator ion. For $Li_2Zr(PO_4)_2$ host, V= 1516.13 $Å^3$, x_c = 0.02, Z = 6. Using formula (2), the value of R_c is calculated to be 28.90 Å. The non-radiative energy transfer mechanism consists of two types: exchange (R_c < 5 Å) or multi - polar interaction (R_c > 5 Å). In the present case (R_c > 5 Å), the non- radiative energy migration between the activator (Dy^{3+}) ion is mainly attributed to the multpole- multipole interaction in $Li_2Zr(PO_4)_2$:Dy^{3+} phosphor. In addition, according to Dexter's theory, the emission intensity per activator ion is presented by the following expression [21]:

$$\frac{I}{x} = \kappa\left[\left(1+\beta(x)^{\theta/3}\right)\right]^{-1} \quad (3)$$

where, x is the concentration of Dy^{3+} ions with $x \geq x_c$, I is the emission intensity, k and β are constants for a given host, θ is the interaction between activator ions and θ = 3, 6, 8 or 10 stands for exchange interaction, dipole–dipole (d–d), dipole-quadrupole (d–q) or quadrupole–quadrupole (q–q) interactions, respectively [22]. The above expression (3) can also be simplified to following expression:

$$\log\left(\frac{I}{x}\right) = A - \frac{\theta}{3}\log(x), \quad A = \log(k) - \log(\beta) \quad (4)$$

Applying the above expression (4), the plot of log(I/x) versus log(x) is presented in Fig. 8. Hence, the value of θ is calculated to be 4.56, which is nearly equal to 6. Hence, the result clearly indicates that the CQ mechanism follows dipole–dipole in $Li_2Zr(PO_4)_2$: Dy^{3+} phosphor.

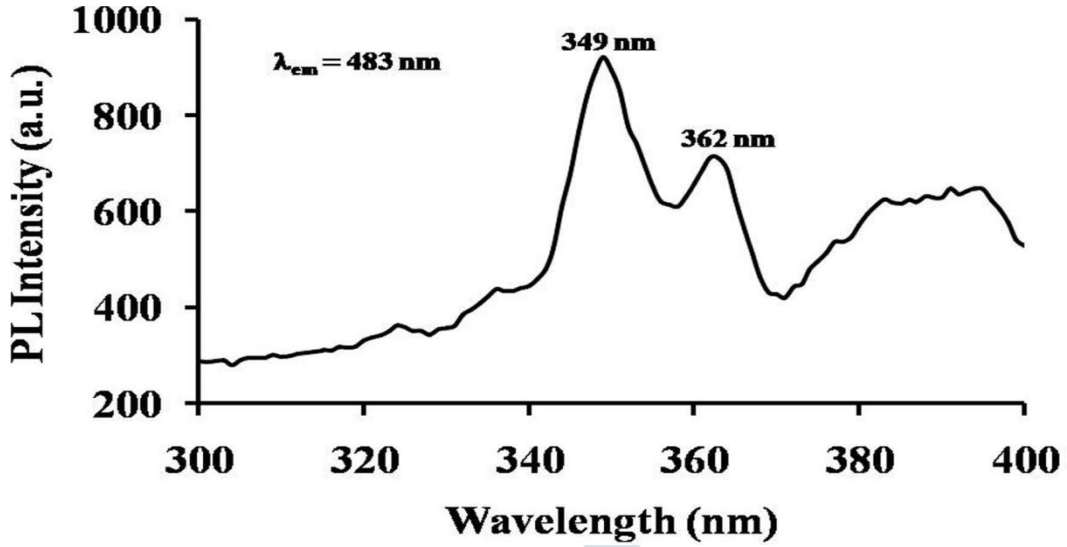

Fig. 5. PL excitation spectrum of $Li_2Zr(PO_4)_2:Dy^{3+}$ (2 mol%) phosphor.

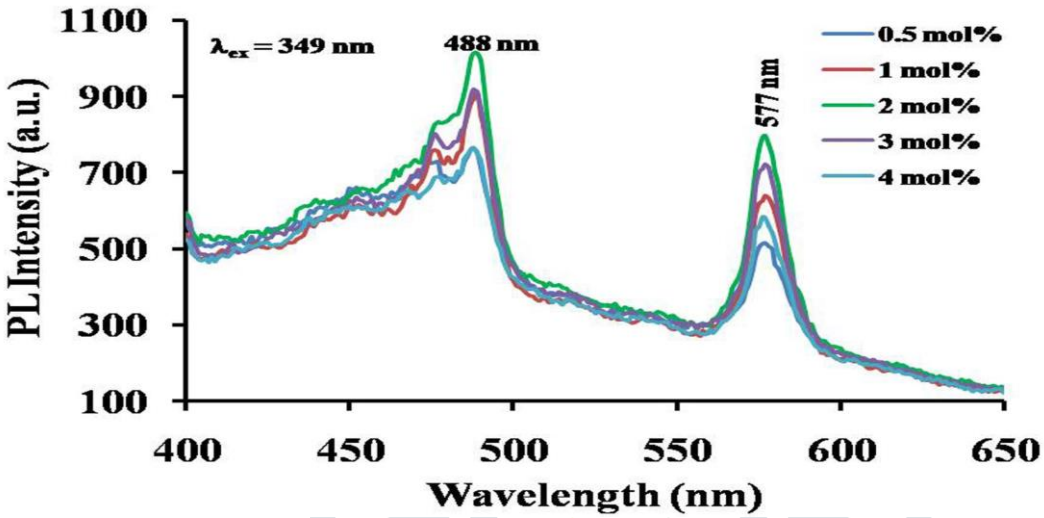

Fig. 6. PL emission spectra of $Li_2Zr(PO_4)_2:Dy^{3+}$ monitored at λ_{ex} = 349 nm.

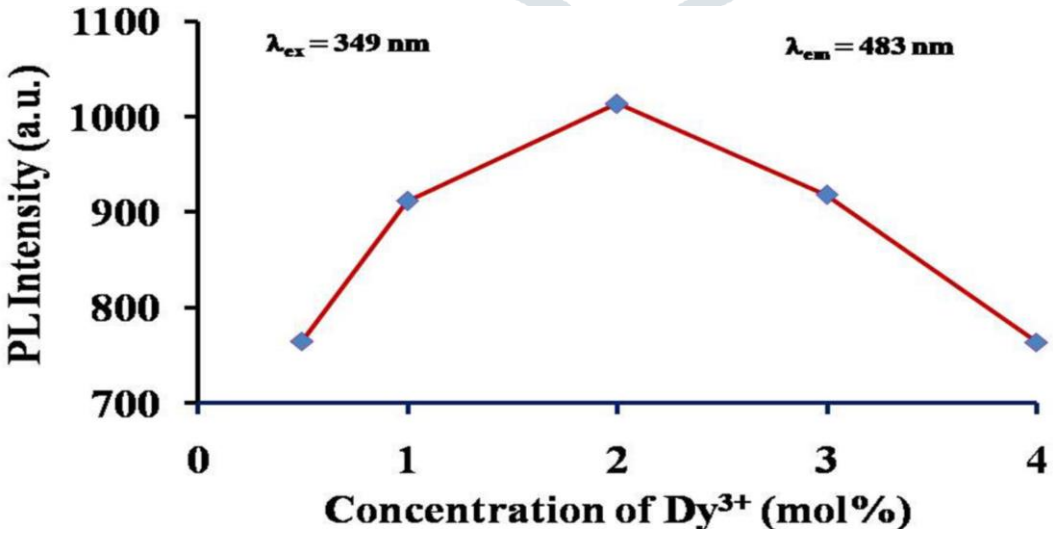

Fig. 7 PL intensity as a function of Dy^{3+} ions in $Li_2Zr(PO_4)_2:Dy^{3+}$ phosphors.

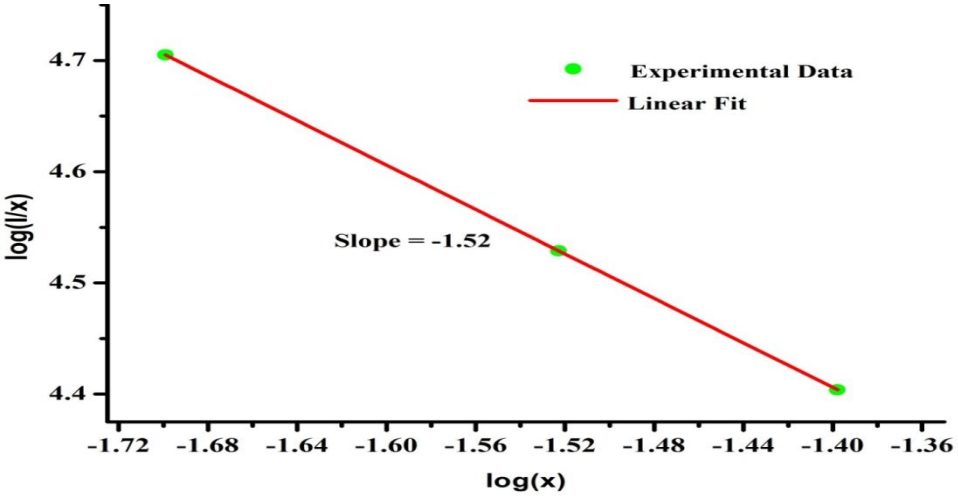

Fig. 8. Graph between log(I/x) and log(x) in $Li_2Zr(PO_4)_2:Dy^{3+}$ phosphors.

3.5 CIE chromaticity co-ordinates

The color of the prepared phosphor excited under 349 nm was characterized by the CIE (Commission International de I'Eclairage) 1931 chromaticity diagram. The emission spectrum of the $Li_2Zr(PO_4)_2:Dy^{3+}$ (2 mol%) phosphor was converted to the CIE 1931 chromaticity using the photoluminescent data and the interactive CIE software (CIE coordinate calculator) diagram as shown in Fig. 9. The luminescence colors of $Li_2Zr(PO_4)_2:Dy^{3+}$ (2 mol%) phosphor are placed in (x = 0.2697, y = 0.3005), which is represented by the circle symbol [''o'']. The CCT value is calculated and found to be 10338 K by using the McCamy's empirical formula [23].

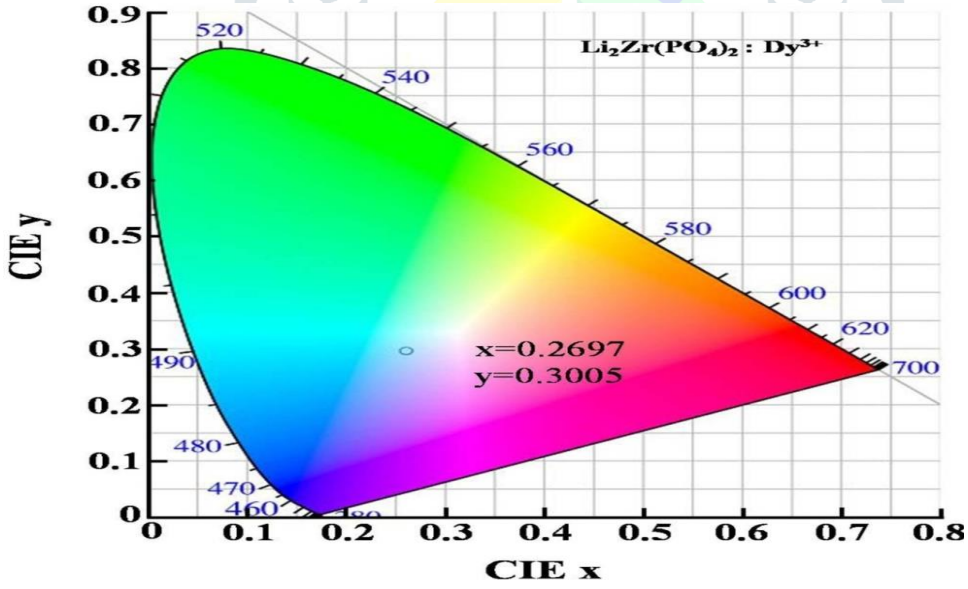

Fig. 9. CIE chromatic diagram of $Li_2Zr(PO_4)_2:Dy^{3+}$ phosphor.

3.6. Decay curve analysis

Fig. 10 shows the decay profile of the prepared $Li_2Zr(PO_4)_2:Dy^{3+}$ (2 mol%) phosphor. The decay curve is recorded at 349 nm excitation and 483 nm emission wavelengths.

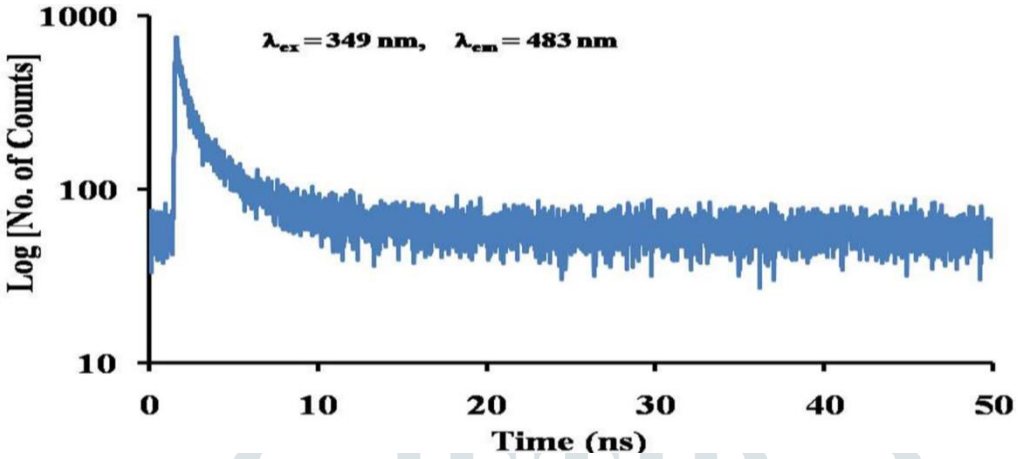

Fig. 10. Decay profile of $Li_2Zr(PO_4)_2:Dy^{3+}$ phosphor.

The initial afterglow intensity of the sample was high. The decay times of phosphor can be calculated by a curve fitting technique, whereas the life time can be so by the relation given below [24]:

$$I = I_1\exp(-t/\tau_1) + I_2\exp(-t/\tau_2) \quad (5)$$

where I_1 and I_2 are two constants, τ_1 and τ_2 are the fast and slow decay times, respectively. The decay times of prepared phosphor were calculated to be as 5.66 ns and 748.92 ns for fast and slow decay process, respectively.

4. CONCLUSIONS

$Li_2Zr(PO_4)_2:Dy^{3+}$ phosphors have been successfully prepared by conventional solid state reaction (SSR) technique. The phase structure, surface morphology and elemental composition of un-doped and Dy^{3+} doped $Li_2Zr(PO_4)_2$ phosphors were determined by the XRD, scanning electron microscopy (SEM) coupled with EDX respectively. The emission spectra of the $Li_2Zr(PO_4)_2:Dy^{3+}$ exhibit two characteristic emission peaks at wavelength 488 nm (blue emission) which corresponds to the magnetic dipole (MD) transition $^4F_{9/2} \rightarrow {}^6H_{15/2}$ and at 577 nm (yellow emission) ascribed to the electric dipole (ED) transition $^4F_{9/2} \rightarrow {}^6H_{13/2}$ with respect to Dy^{3+} ion. The ED transition is dominated in the emission spectra when Dy^{3+} ion is located at a low symmetry site and the MD transition is dominated when Dy^{3+} ion is located at high symmetry sites. The maximum PL intensity was obtained at 2 mol % of dopant Dy^{3+} ions. The CIE coordinates were originated (0.2697, 0.3005) for $Li_2Zr(PO_4)_2:Dy^{3+}$ (2 mol%) phosphor and the CCT value was calculated to be as 10338 K. The luminescence decay times were found to be 5.66 ns and 748.92 ns for fast and slow decay process. The investigated results indicate that prepared phosphor could be a suitable component for light emitting devices.

5. REFERENCES

[1] H. A. Höppe, 2009. Recent Developments in the Field of Inorganic Phosphors, Angew. Chem. Int. Ed., 48 (20), 3572-3582.

[2] T. Chan, R. Liu and I. Baginskiy, 2008. Synthesis, Crystal Structure, and Luminescence Properties of a Novel Green-Yellow Emitting Phosphor $LiZn_{1-x}PO_4:Mn_x$ for Light Emitting Diodes, Chem. Mater., 20, 1215-1217.

[3] Y. Tang, S. Hu, C. Lin, N. C. Bagkar and R. Liu, 2007. Thermally stable luminescence of $KSrPO_4:Eu^{2+}$ phosphor for white light UV light-emitting diodes, J. Appl. Phys. Lett., 90, 151108-1-3.

[4] C. C. Lin, Y. S. Tang, S. F. Hu and R. S. Liu, 2009. $KBaPO_4$:Ln (Ln = Eu, Tb, Sm) phosphors for UV excitable white light-emitting diodes, J. Lumin., 129, 1682-1684.

[5] J. Kuang and Y. Liu, 2005. White-emitting Long-lasting Phosphor $Sr_2SiO_4:Dy^{3+}$, Chem. Lett. 34, 598-599.

[6] D. Jia and W. M. Yen, 2003. Enhanced V_K^{3+} center afterglow in $MgAl_2O_4$ by doping with Ce^{3+}, J. Lumin., 101, 115-121.

[7] M. Yu, J. Lin, Z. Wang, J. Fu, S. Wang, H. J. Zhang and Y. C. Han, 2002. Fabrication, Patterning, and Optical Properties of Nanocrystalline YVO_4:A (A = Eu^{3+}, Dy^{3+}, Sm^{3+}, Er^{3+}) Phosphor Films via Sol−Gel Soft Lithography, Chem. Mater., 14, 2224-2231.

[8] R. Ravichandran, S. T. Johnson, S. Erdei, R. Roy and W. B. White, 1999. Crystal chemistry and luminescence of the Eu^{2+}-activated alkaline earth aluminate phosphors, Displays, 19, 197-203.

[9] B. Smets, J. Rutten, G. Hoeks, and J. Verlijsdonk, 1989. $2SrO\cdot 3Al_2O_3:Eu^{2+}$ and 1.29 (Ba, Ca)O, $6Al_2O_3:Eu^{2+}$:Two New Blue-Emitting Phosphors, J. Electrochem. Soc. 136, 2119-2123.

[10] T. Katsumata, K. Sasajima, T. Nabae, S. Komuro and T. Morikawa, 1998. Characteristics of Strontium Aluminate Crystals Used for Long-Duration Phosphors, J. Am. Ceram. Soc. 81, 413-416.

[11] J. L. Sommerdijk and A. Bril, 1975. Efficiency of Dy^{3+}-Activated Phosphors, J. Electrochem. Soc, 122, 952-954.

[12] J. S. Kim et al., 2005. Full-color $Ba_3MgSi_2O_8:Eu^{2+}$, Mn^{2+} phosphors for white-light-emitting diodes, Solid State Commun., 135, 21-24.

[13] O. Nazari et al. 2019. Synthesis and characterization of cadmium selenide quantum dots doped by europium and investigation of their chemiluminescence properties and antibacterial activities, Luminescence, 34, 394-401.

[14] K. Munirathnam, et al. 2015. Synthesis, photoluminescence and Judd–Ofelt parameters of $LiNa_3P_2O_7:Eu^{3+}$ orthorhombic microstructures, Appl. Phys. A, 120, 1615-1623.

[15] D.E. Corbridge, 1966. Topics in Phosphorus Chemistry, ed. by M. Grayson, E.J. Griffith, New York, 275.

[16] R. L. Kohale, S. J. Dhoble, 2014. Synthesis and influence of Ce^{3+} co-dopant on the luminescence sensitivity of $SrZnP_2O_7:Dy^{3+}$ phosphor, J. Alloys Compd., 586, 314-318.

[17] I. M. Nagpure, V. B. Pawade, S. J. Dhoble, 2010. Combustion synthesis of $Na_2Sr(PO_4)F:Dy^{3+}$ white light emitting phosphor, Luminescence, 25, 9-13.

[18] L. Li et al., 2015. Investigation on white light emissions from CeO_2/Dy_2O_3 multilayer films based on silicon substrates, Vacuum, 112, 38-41.

[19] K. N. Shinde, S. J. Dhoble, A. Kumar, 2011. Synthesis of novel Dy^{3+} activated phosphate phosphors for NUV excited LED, J. Lumin., 131, 931-937.

[20] G. Blasse, 1986. Energy transfer between inequivalent Eu^{2+} ions, J. Solid State Chem., 62, 207–211.

[21] J. Fan et al., 2018. Effect of charge compensators A^+ (A = Li, Na and K) on luminescence enhancement of $Ca_3Sr_3(PO_4)_4:Sm^{3+}$ orange-red phosphors, Ceram. Int., 44, 20028-20033.

[22] P. Du, L. K. Bharat, X. Y. Guan, J. S. Yu, 2015. Synthesis and luminescence properties of color-tunable Dy^{3+}-activated $CaWO_4$ phosphors, J. Appl. Phys., 117(8), 083112-1-6.

[23] C. S. McCamy, 1992. Correlated color temperature as an explicit function of chromaticity coordinates, Color Res. Appl., 17, 142-144.

[24] M. Shoaib, et al. 2019. Luminescence properties of Nd^{3+} ions doped P_2O_5-Li_2O_3- GdF_3 glasses for laser applications, Optik, 199, 163218-1-7.